Atmos. Chem. Phys. Discuss., 11, 12519–12560, 2011
www.atmos-chem-phys-discuss.net/11/12519/2011/
doi:10.5194/acpd-11-12519-2011
© Author(s) 2011. CC Attribution 3.0 License.

Atmospheric Chemistry and Physics Discussions

This discussion paper is/has been under review for the journal Atmospheric Chemistry and Physics (ACP). Please refer to the corresponding final paper in ACP if available.

A multi-angle aerosol optical depth retrieval algorithm for geostationary satellite data over the United States

H. Zhang[1], A. Lyapustin[2], Y. Wang[2], S. Kondragunta[3], I. Laszlo[3], P. Ciren[4], and R. M. Hoff[1,2]

[1]Joint Center for Earth Systems Technology (JCET), University of Maryland Baltimore County, Suite 320, 5523 Research Park Drive, Baltimore, MD 21228, USA
[2]Goddard Earth Sciences and Technology Center (GEST), University of Maryland Baltimore County, Suite 320, 5523 Research Park Drive, Baltimore, MD 21228, USA
[3]NOAA/NESDIS/STAR, 5825 University Research Ct, College Park, MD 20740, USA
[4]PSGS/Dell, 5825 University Research Ct, College Park, MD 20740, USA

Received: 29 October 2010 – Accepted: 14 April 2011 – Published: 20 April 2011

Correspondence to: H. Zhang (hazhang@umbc.edu)

Published by Copernicus Publications on behalf of the European Geosciences Union.

Abstract

Aerosol optical depth (AOD) retrieval from geostationary satellites has high temporal resolution compared to the polar orbiting satellites and thus enables us to monitor aerosol motion. However, current Geostationary Operational Environmental Satellites (GOES) have only one visible channel for retrieving aerosol and hence the retrieval accuracy is lower than those from the multichannel polar-orbiting satellite instruments such as the Moderate Resolution Imaging Spectroradiometer (MODIS). The operational GOES AOD retrieval algorithm (GOES Aerosol/Smoke Product, GASP) uses 28-day composite images from the visible channel to derive surface reflectance, which can produce large uncertainties. In this work, we develop a new AOD retrieval algorithm for the GOES imager by applying a modified multi-angle Implementation of Atmospheric Correction (MAIAC) algorithm. The algorithm assumes the surface Bidirectional Reflectance Distribution Function (BRDF) at channel 1 of GOES is proportional to seasonal average BRDF in the 2.1 µm channel from MODIS. The ratios between them are derived through time series analysis of the GOES visible channel images. The results of the AOD and surface reflectance retrievals are evaluated through comparison against those from Aerosol Robotic Network (AERONET), GASP, and MODIS. The AOD retrievals from the new algorithm demonstrate good agreement with AERONET retrievals at several sites across the US. They are comparable to the GASP retrievals in the eastern-central sites and are more accurate than GASP retrievals in the western sites. In the western US where surface reflectance is high, the new algorithm also produces larger AOD retrieval coverage than both GASP and MODIS.

1 Introduction

Aerosols play an important role in the atmosphere by modifying radiative forcing and air quality. They can affect the climate by directly changing the radiation reflected from the Earth and can also indirectly change the radiative forcing at the top of atmosphere (TOA) by modifying the cloud properties through microphysical process (Charlson et

ACPD
11, 12519–12560, 2011

al., 1992; Kiehl et al., 1993). In addition, aerosols also influence the air quality close to the surface and affect the human health (Pope et al., 2002, 2006; Chow et al., 2006). Thus, accurate measurements of aerosols can both improve our knowledge on climate change (Intergovernmental Panel on Climate Change, 2007) and improve our ability to monitor and to forecast particulate matter air quality (e.g. Al-Saadi et al., 2005; Hoff and Christopher, 2009; Hidy et al., 2009).

Many polar orbiting satellite instruments are used to measure aerosols, such as MODIS (Kaufman et al., 1997; Tanré et al., 1997; Levy et al., 2007), Multiangle Imaging Spectroradiometer (MISR) (Martonchik et al., 1998), POLarization and Directionality of the Earth's Reflectances (POLDER, Deuzé et al., 2001) etc., but they all have low temporal resolution. For example, the widely used aerosol product from MODIS only has a twice-daily coverage from Terra and Aqua platform. Geostationary satellites can overcome this shortcoming: the National Oceanic and Atmospheric Administration (NOAA) GOES makes the monitoring of aerosols available at a higher temporal resolution over the United States with a rate of every half hour during sun-lit period (Prados et al., 2007). However, current GOES only has one visible channel that can be used for retrieving AOD, which makes the uncertainty of retrievals larger than those from MODIS that utilizes multi-spectral signal for the AOD retrieval (Prados et al., 2007).

The current operational GASP product uses 28-day composite image from channel 1 (visible channel with spectral range of 0.52–0.72 µm) to find the second darkest day at each observation time and uses it to retrieve surface reflectance. The GASP algorithm assumes that the surface reflectance does not change during the 28-day period and that AOD at the second darkest day is 0.02. The uncertainties of GASP originate from assumptions of aerosol model, surface reflectance, cloud/cloud shadow contamination, and calibration errors. The uncertainty in the surface reflectance retrieval may result in large error in AOD retrievals. First, during the 28-day period for surface reflectance retrieval, the surface property may change due to the change in the color and growing state of vegetation. Second, the surface reflectance may also be different between the day of AOD retrieval and the day of surface reflectance retrieval because of the

ACPD
11, 12519–12560, 2011

difference in solar angles between these two days. Thirdly, the existence of cloud shadow may introduce too low surface reflectance retrieval at the times when cloud shadow occurs frequently. In addition, the look-up-table (LUT) in GASP is generated from 6S with Lambertian assumption. The ignorance of non-Lambertian nature of surface may generate large errors in some situations. The motivation of this research is to develop a new algorithm that can retrieve surface reflectance more accurately by reducing the period for surface reflectance retrieval. In this new method, we abandon the Lambertian assumption and make use of BRDF to model the surface property in order to reduce the uncertainty in surface reflectance retrievals.

The MAIAC algorithm is an aerosol retrieval and atmospheric correction scheme over land for MODIS data developed by Lyapustin and Wang (2009). The algorithm uses time series of multi-channel images to retrieve surface BRDF and aerosol properties. The surface BRDF is first retrieved in the 2.12 µm band assuming this band is not affected by aerosol. Then surface BRDF in the blue band and the red band are assumed to be proportional to that in the 2.12 µm band, and the ratios are retrieved from time series analysis with the aid of look-up-table (LUT) generated from a radiative transfer model. The benefit of this method is that it can be applied to regions where the surface reflectance relations between blue, red and SWIR band in MODIS operational retrieval algorithm (MOD04) are inaccurate. For example, MAIAC algorithm can retrieve AOD over bright surfaces such as desert where MOD04 does not have retrievals. In this paper, we modify this algorithm so that it can use GOES data to retrieve surface BRDF and AOD. Since current GOES does not contain a SWIR band, we use seasonal averages of MODIS BRDF in the 2.12 µm band for reference, and assume that BRDF in the GOES visible band is proportional to MODIS BRDF at 2.12 µm. The MAIAC algorithm can hence be applied for aerosol retrieval using GOES visible band data.

In Sect. 2, we describe the data used in this work. In Sect. 3, we describe the details of the modified MAIAC algorithm. In Sect. 4, we evaluate the retrieval results through comparison to AERONET, GASP and MODIS retrievals. In Sect. 5, we conclude the work.

ACPD
11, 12519–12560, 2011

2 Data

2.1 GOES data

The current GOES satellite imager measures radiances reflected and emitted from the Earth and atmosphere in one visible channel and four infrared channels. In this study, we use channel 1 (visible channel, 0.52–0.72 µm), channel 2 (3.9 µm) and channel 4 (10.7 µm) radiances from GOES-12, which is located at 75°W above the equator. The visible channel radiances are used for surface reflectance and AOD retrieval and the two infrared channels radiances are used for deriving cloud masks. The spatial resolution at nadir is 1 km for the visible channel and is 4 km for the IR channels. Since there is no on-board calibration device for the imager, the radiances are calibrated using a vicarious method (see http://www.oso.noaa.gov/goes/goes-calibration/goes-vis-ch-calibration.htm). GOES-12 images covering continental US have a temporal resolution of half hour.

To evaluate the retrieval results of the MAIAC algorithm, we compare the results with those from the current operational algorithm: GASP (Knapp et al., 2005; Prados et al., 2007). GASP provides AOD retrievals at 0.55 µm with a spatial resolution of 4 km. As mentioned above, it uses a 28-day composite image of visible channel to derive surface reflectance with an assumption of 0.02 background AOD on the second clearest day. The retrieved surface reflectance is used along with channel 1 radiances and the LUT from 6S radiative transfer model to retrieve AOD. The cloud-masking algorithm is based on CLAVR (Clouds from AVHRR) algorithm from AVHRR (Advanced Very High Resolution Radiometer) (Stowe et al., 1999; Heidinger et al., 2001).

2.2 AERONET data

AERONET (http://aeronet.gsfc.nasa.gov) is a global network for aerosol monitoring from ground stations using Sunphotometers. The quality assured level 2.0 AERONET AOD data is used for evaluating the AOD retrievals and for evaluating the surface BRDF

ACPD
11, 12519–12560, 2011

retrievals from GOES data. Since the AERONET AOD retrievals have an accuracy of ±0.02 (Holben et al., 1998), they can be treated as ground truth. Since AERONET AOD does not measure at wavelength 0.55 µm, we calculate it through log-linear interpolation from two nearest wavelengths, i.e. 0.5 µm and 0.675 µm. We select six AERONET sites across continental US for the validation of MAIAC algorithm. Table 1 summarizes the locations of the AERONET sites used for the validation in this work and Fig. 1 shows their locations on the map of the United States.

2.3 MODIS data

MODIS BRDF (Lucht et al., 2000) in the band 2.12 µm is used as an aid for the retrieval of surface BRDF from GOES visible channel radiances. Here, BRDF is modeled by RossThick-LiSparse model (Roujean et al., 1992), which contains three parts, including isotropic, geometric and volumetric scattering reflectance, as shown in the following equation:

$$\rho(\theta_s,\theta_v,\phi) = k_{\text{iso}} + k_{\text{geo}} f_{\text{geo}}(\theta_s,\theta_v,\phi) + k_{\text{vol}} f_{\text{vol}}(\theta_s,\theta_v,\phi) \quad (1)$$

where $\rho(\theta_s,\theta_v,\phi)$ is BRDF, k_{iso}, k_{geo}, and k_{vol} are the weights for the three components and f_{geo} and f_{vol} are kernel functions for geometric and volumetric components, respectively. The three BRDF weight parameters (k_{iso}, k_{geo}, k_{vol}) in the 2.1 µm band are obtained from the MODIS level 2 land products MCD43D19, MCD43D20, and MCD43D21 with a spatial resolution of 1km. These BRDF parameters are retrieved using 16 days of MODIS measurements and are updated every eight days.

MODIS level 2 aerosol optical depth product from Terra and Aqua is used for comparison with the AOD retrievals from GOES. The MODIS aerosol retrieval algorithm over land uses three bands, i.e. blue band, red band, and SWIR band (2.12 µm), to derive the aerosol properties with a 10 km resolution (Levy et al., 2007).

ACPD
11, 12519–12560, 2011

3 Aerosol optical depth retrieval algorithm

One of the challenges in the satellite aerosol optical depth retrieval is the separation of the contributions from surface reflectance and aerosol reflectance to the radiances at top of the atmosphere (TOA). As mentioned previously, the retrieval of surface reflectance in GASP makes use of 28-day composite images at a specific observation time with an assumption that the surface reflectance does not change. However, due to the change of the solar zenith angle and the change of surface vegetation during these 28 days, the surface reflectance may vary a lot, which may create large uncertainties in the AOD retrieval. For example, we observed a change from 0.11 to 0.14 in a 28-day period at 1645 UTC at GSFC site in the fall. An underestimate of surface reflectance of 0.03 can produce an AOD overestimate as large as 0.6. If we can reduce the number of days involved in the surface reflectance retrieval and use a more realistic BRDF model for surface reflectance retrieval, the uncertainties due to the surface reflectance retrieval may be reduced. Surface reflectance obtained from GASP algorithm may also be affected by cloud shadows and the assumption of 0.02 background AOD in the second clearest day of the 28-day time sequence.

The algorithm in this work applies the MAIAC algorithm designed for MODIS to the retrieval of AOD from GOES imager data. The algorithm makes following three assumptions: (1) BRDF in the GOES visible band is proportional to BRDF in the MODIS 2.12 µm band, i.e. the BRDF shapes are the same in these two bands; (2) the BRDF shape does not change much within a season so that we can use a seasonal average of 2.12 µm band BRDF from MODIS to represent BRDF shape for each season; (3) since the mesoscale range of the aerosols is about 50–60 km (Anderson et al., 2003), aerosol is assumed to distribute uniformly over a distance of 24 km. We assume AOD to be constant in each $24 \times 24\,km^2$ block when we do time series analysis for surface BRDF retrieval.

Before applying the AOD retrieval algorithm, we perform an image co-registration for the images from GOES imager, since we found that the GOES images shift from time to

ACPD
11, 12519–12560, 2011

time due to the jitter of the satellite orbit and a relatively low image navigation accuracy (4 km at nadir, GOES I-M databook, 1996). To do this, we generate a reference image by projecting the MODIS average surface reflectance image onto the GOES channel 1 grid. All the input GOES channel 1 images will be compared against this reference image to correct the shifts. We select more than one hundred control points along the coastlines in such a way that the areas around the control points have high contrast and contain features that are suitable for pattern matching using a correlation method. For example, island and area with complex coastlines are good places for setting up the control points. The input GOES channel 1 images are compared against the reference image at each control point. A small window is selected around the control point to be used to determine the image shift there. The GOES image from the small window is shifted iteratively and the correlation coefficient with the reference image at each shift position is calculated. If the GOES image within the small window is free from cloud, a correlation peak can be found when the small window area is colocated with the reference image. Therefore, the satellite image shift at the control point is determined to be the value at which the maximum correlation is found. If the GOES image within the window is covered by cloud, we will not be able to find a large correlation with the reference. Thus, we require the maximum correlation be larger than 0.7 to be an effective shift calculation. To determine the shift over the whole image, we assume the shifts vary linearly with respect to the location:

$$\Delta x(i,j) = Ai + Bj + C, \tag{2}$$

$$\Delta y(i,j) = Di + Ej + F, \tag{3}$$

where $\Delta x(i,j)$ and $\Delta y(i,j)$ is the shifts in x and y direction at pixel with index (i,j), A, B, C, D, E, F are coefficients to be determined. Since the value of $\Delta x(i,j)$ and $\Delta y(i,j)$ at the control points free from clouds have already been determined above, we can calculate these coefficients through linear regression.

After image co-registration, the MAIAC retrieval algorithm for surface BRDF and AOD is applied. The algorithm flowchart is shown in Fig. 2. The GOES channel 1, 2, and

ACPD
11, 12519–12560, 2011

4 images are placed in a queue sorted by the time of acquisition for processing. We use the CLAVR algorithm for cloud mask, which is the same as the one used in GASP retrieval scheme. Since the resolutions of two IR channels are 4 km, we break each pixel into 4 × 4 pixels with 1 km in size and assign each of the new pixels with the same value as the original one. With such arrangement, CLAVR algorithm can be applied at 1 km resolution. In addition, we also apply the following criterion to determine cloud pixels that fail to be masked in CLAVR algorithm: if the standard deviation of a 3 × 3 box surrounding a pixel in channel 1 TOA reflectance is greater than 0.015, the pixel is also marked as cloudy, which is similar to the MODIS cloud mask algorithm by Martins et al. (2002).

After cloud masking, the 1 km resolution grids are grouped into blocks with size 24 × 24. Surface BRDF at each pixel is derived through retrieving the spectral regression coefficients (SRC) between MODIS 2.12 µm BRDF and GOES channel 1 BRDF. Here, SRC is defined as the ratio between GOES channel 1 band BRDF and MODIS 2.12 µm band BRDF. We perform SRC retrieval if there are at least three cloud free blocks in the time sequence. For each pixel within a block, we calculate the SRC with the assumption that AOD is 0. A block is considered to be clearest if its average SRC is the lowest in the time sequence. Next, the AOD difference between each block and the clearest block is determined by looking for the AOD difference that minimizes the difference between SRCs from these two observations, i.e. the AOD difference is $\Delta\tau^k$ that minimizes $\frac{1}{N}\sum_{i,j}\{b_{ij}^{\text{clearest}} - b_{ij}^k(\Delta\tau^k)\}^2$, where N is the number of pixels that are cloud free in both the clearest image block and the image block for comparison (k), b_{ij}^{clearest} is SRC at the clearest time for pixel with indices i and j, $b_{ij}^k(\Delta\tau^k)$ is the SRC at observation k for pixel with indices i and j if the AOD difference between image block k and the clearest image block is $\Delta\tau^k$.

After the AOD differences are calculated, we calculate AOD at the clearest observation, which is obtained by looking for the AOD value that minimizes the root mean square differences between the theoretical TOA radiance and the measured TOA radiance for all the blocks in the queue, i.e. looking for τ_0 that minimizes the quantity

ACPD
11, 12519–12560, 2011

$\sum_k \sum_{i,j} \{R_{ij}^{\mathrm{Meas},k} - R_{ij}^{Th,k}(\tau_0 + \Delta\tau^k)\}^2$, where $R_{ij}^{\mathrm{Meas},k}$ is the measured radiance at pixel (i,j) for image block k, $R_{ij}^{Th,k}(\tau_0 + \Delta\tau^k)$ is the theoretical radiance at this pixel for image block k if AOD for the clearest image is τ_0. AOD derived at this step is the average AOD over the whole block to help retrieve surface BRDF.

After deriving AOD at the clearest observation, we use it to retrieve the SRC and surface BRDF at each pixel within the block. To retrieve AOD at a higher resolution, we regroup GOES channel 1 image into 4×4. If the total number of cloud free pixels in a group is greater than 8, i.e. more than half of the pixels are cloud free, we retrieve AOD in this group using average TOA reflectance and average surface BRDF of the cloud free pixels.

To illustrate the implementation of the algrotihm, we plot a data flow diagram in Fig. 3. The incoming image is divided into blocks with size $24 \times 24\,\mathrm{km}^2$. Since channel 1 and channel 2,4 have different resolution, their dimension in terms of pixels are different, i.e. 6×6 for channel 2 and 4. As discribed above, we break each pixel of channel 2 and 4 into 4×4 pixels with $1\,\mathrm{km}^2$ resolution so that blocks of channel 2 and 4 have the same dimension as those of channel 1. After cloud mask, channel 2 and channel 4 data are no longer used. Channel 1 data, geometry data, along with cloud mask are inserted into the end of a First In First Out (FIFO) queue for BRDF. At the same time, the beginning block of the queue is removed. We set the length of the queue to be 16. The data blocks in the queue include time sequence of GOES observations for the same area. BRDF for this block area is derived from the method described above. The AOD is then derived from BRDF and the latest channel 1 data in resolution of 4 km, i.e. 6×6 in terms of pixels.

The retrieval algorithm described above is implemented with the aid of a look-up-table (LUT). Unlike GASP, in which Lambertian 6S radiative transfer model (Vermote et al., 1997) is used to generate LUT, we use non-Lambertian SHARM model (Lyapustin and Knyazikhin , 2001; Lyapustin and Wang, 2005). In this model, the reflectance at the top of the atmosphere (ρ) can approximately be written as (Lyapustin and Wang, 2008):

ACPD
11, 12519–12560, 2011

$$\rho = \rho^D(\tau) + b[k_{\text{iso}}^{B7} F_{\text{iso}}(\tau) + k_{\text{geo}}^{B7} F_{\text{geo}}(\tau) + k_{\text{vol}}^{B7} F_{\text{vol}}(\tau)], \quad (4)$$

where ρ^D represents the atmospheric path reflectance, b is the SRC between GOES channel 1 and MODIS 2.1 µm band BRDF, k_{iso}^{B7}, k_{geo}^{B7}, k_{vol}^{B7} are weights of BRDF in the MODIS 2.1 µm band, F_{iso}, F_{geo}, F_{vol} are reflectance contribution from isotropic, geometric and volumetric part of surface BRDF, respectively. The detailed expressions of F_{iso}, F_{geo}, F_{vol} can be found in Lyapustin and Wang (2008). In LUT, we save ρ^D and functions to calculate F_{iso}, F_{geo}, F_{vol} for different sun-satellite geometry and AOD combinations.

We use an aerosol model with fine and coarse fractions in lognormal distribution with following parameters: $R_v = 0.14$ µm, 3.2 µm, $\sigma_v = 0.35$ µm, 0.7 µm, $n_r = 1.45$, $n_i = 0.006$. The ratio of volumetric concentrations between the coarse and fine mode is $Cv_{\text{coarse}}/Cv_{\text{fine}} = 0.5$. This model is similar to the aerosol model from AERONET at GSFC. We use climatological values of column ozone and water vapor for gaseous absorption calculation since their variations do not introduce much variation on the surface reflectance and AOD retrievals (Knapp et al., 2002; Zhang et al., 2008).

4 Results and validation

4.1 Image co-registration

Figure 4 shows an example result of image co-registration. The top two pictures are image portionss with coastlines from channel 1 with 1 km resolution taken at different times over the same area at long island of New York. The pixels with same indices from the two images have the same latitude and longitude derived from the GOES channel 1 navigation algorithm. We can see that the two images have a relative shift of about two pixels. If we subtract the two images, shown in the bottom left, the coastlines appear to have higher or lower values than the surroundings due to the shift between the two images. The bottom right image shows the same subtraction of the two sub-images

ACPD
11, 12519–12560, 2011

after image co-registration. The higher or lower values along the coastlines are almost removed, indicating that the image co-registration process reduces the shift between the two images to less than one pixel.

To find the optimal window size at the control point, we tested several different values. Figure 5 shows several statistics of these tests, including RMSE of the image shift after image co-registration, number of effective control points, and the maximum correlation. We can see that with the increase in the window size, RMSE becomes smaller; however, the number of effective control points is also reduced with increased window size. The maximum correlation is centered at 0.83 for the window size from 20 to 50. In our following study, we use a size of 40×40 in order to compromise between RMSE and number of effective control points.

4.2 Comparison of AOD retrieval against AERONET and GASP

The AOD retrieval results are compared to the AERONET measurements at the six AERONET sites over the United States described in Sect. 2.2. To find the coincidence between GOES AOD retrieval and AERONET measurements, we use the average GOES AOD retrievals within 5×5 box surrounding the AERONET site and the interpolation of two closest AERONET measurements within 15 minutes before and after GOES observation. In cases where only one AERONET measurement is available within ± 15 minutes time frame, we use that value instead of interpolation. To further remove cloud contamination, we remove the pixels adjacent to cloud, require more than 10 effective pixels in the 25 pixels, and require standard deviation of AOD in the 5×5 box is less than 0.2. We also use two additional filters for backscatter geometry and bright surface, which are described in the following two subsections. GASP data are prepared using average in 5×5 box surrounding the AERONET site and are applied the filters described in Prados et al. (2007). In addition, GASP data also uses a standard deviation threshold of 0.2 for cloud contamination removal. Because of the difference in the retrieval and screening algorithm, the coincidences of AOD retrievals

ACPD
11, 12519–12560, 2011

are not exactly the same between MAIAC and GASP. The dataset covers the period between 1 March 2008 and 25 September 2008.

4.2.1 Backscatter geometry

At backscatter geometry where the Sun is located directly at the back of the satellite, we notice large bias in the AOD retrievals. Figure 6 shows the AOD retrieval errors vs. scatter angle at GSFC site. We can see that the errors increase systematically when scatter angle increases above 160°. The backscatter geometry corresponds to the location of hot spot where surface BRDF is the highest. Such errors are caused by the large errors of MODIS BRDF close to the hot spot. MODIS BRDF retrievals do not model the hot spot well if MODIS do not sample at the positions close to the hot spot at backscatter geometry. We can also see that the errors are relative small at scatter angles below 160°, which indicate that MODIS BRDF works well away from hot spot. In the following validation, we remove the AOD retrievals with scatter angle larger than 160°. In GASP, most retrievals at such geometries are also removed due to high surface reflectance since GASP filters out pixels with surface reflectance larger than 0.15.

4.2.2 Bright surface

In this work, we use a different filter for bright surfaces, which are mostly located in the western US. Railroad Valley site at Nevada is very bright and it is a good site to test the GOES AOD retrieval algorithm at locations with high surface reflectance. The sun-satellite geometries at Railroad Valley can represent typical geometries of western US. Figure 7 shows contours of TOA reflectance as a function of surface reflectance and AOD at three geometry setups at Railroad Valley site: morning (1615 UTC), noon (1915 UTC), and afternoon (2215 UTC). We can see that the 0.2 contour line at noon with surface reflectance close to 0.2 and AOD close to 0 is almost flat, which indicates that a small surface reflectance error can introduce a large AOD error.

ACPD
11, 12519–12560, 2011

Hence AOD uncertainty is high at such geometry and surface reflectance combination. We can also see that at high surface reflectance with some sun-satellite geometry the TOA reflectance decreases even if AOD increases. In such geometry, we may have two solutions of AOD with given TOA reflectance and surface reflectance. Such phenomenon was also observed in previous research by Fraser and Kaufman (1985); Kaufman (1987). However, in the afternoon, the contours are mostly falling downward as AOD increases. So, in the afternoon, the AOD retrieval error should be much less sensitive to errors in surface reflectance. From such observation, the sensitivity of AOD retrieval over surface reflectance is dependent on both the sun-satellite geometry and the value surface reflectance. It is not appropriate to use a uniform threshold of surface reflectance to filter out AOD retrievals with high sensitivity to surface reflectance retrieval.

Based on the above discussion, instead of using fixed surface reflectance threshold, we apply a new filter to remove noisy AOD retrievals due to the errors in surface reflectance. This filter uses $\left|\frac{\partial \tau}{\partial \rho_{sfc}}\right|_{\tau=0}$, with TOA reflectance and sun-satellite geometry fixed, to remove noise due to the surface reflectance retrieval errors. The AOD retrievals are removed if this value is smaller than −20 and larger than 0. Since we can write AOD retrieval error as $\Delta\tau = \frac{\partial \tau}{\partial \rho_{sfc}} \Delta\rho_{sfc}$, if other conditions are not changed, large $\left|\frac{\partial \tau}{\partial \rho_{sfc}}\right|$ value means that large AOD error can be introduced with error in surface reflectance retrieval. If $\frac{\partial \tau}{\partial \rho_{sfc}}$ is positive at 0 AOD, it is possible that the value turns negative at some higher AOD value, which suggests two AOD solutions for the same set of parameters, i.e. ρ_{sfc}, ρ_{TOA} , and three geometric angles.

4.2.3 Validation of AOD retrievals

Figure 8 shows the scatter plots of MAIAC vs. AERONET AOD at the six AERONET sites. For comparison, Fig. 9 shows the corresponding scatter plots of GASP vs. AERONET AOD. MAIAC retrievals have correlation of more than 0.8 at GSFC, Railroad Valley, and UCSB site. MAIAC retrievals have smaller RMSE than GASP retrievals at

ACPD
11, 12519–12560, 2011

all the sites. Because the two retrieval algorithms use different screening scheme to remove noisy data, the numbers of AOD retrievals are different in the two retrieval algorithms. Figure 10 shows the scatter plots with one-to-one correspondence between MAIAC and GASP retrievals. With one-to-one correspondence, MAIAC retrievals have similar correlation with AERONET AOD to the GASP retrievals vs. AERONET AOD at eastern and central sites, i.e. GSFC, Walker Branch, Howland, and Bondville, but MAIAC have smaller RMSE at three of them: GSFC, Walker Branch, and Bondville. At the two western sites, MAIAC AOD retrievals are much more accurate than GASP retrievals in both correlation coefficient and RMSE.

There are several reasons that may increase or decrease the accuracy in the MAIAC algorithm in comparison to GASP. First, MAIAC algorithm requires less number of days to retrieve surface BRDF: normally surface BRDF can be retrieved in one day if three clear observations are found. This can reduce uncertainties in surface BRDF retrieval due to the change in surface BRDF during a period shorter than 28 days, which is used in GASP for surface retrieval. The GASP method tends to pick up cloud shadow in some geometries, e.g. during the afternoon in the western US when the sun shines from the west. Second, in MAIAC, we use a more realistic aerosol model which is similar to that retrieved from GSFC. GASP uses a different aerosol model, i.e. continental model, which has a lower single single scatter albedo, and hence GASP tends to have higher AOD retrievals than MAIAC. Third, the algorithm does not use Lambertian assumption as in GASP. The non-Lambertian effect may be large in some situations, which will be discussed in the following section. Fourth, we use a new screen algorithm at bright surface described in the last section. This screen scheme generates a larger number of retrievals at bright surface than the use of simple threshold of 0.15 surface reflectance. We can see that at Railroad Valley there are more coincidences are available in MAIAC than those in GASP.

The difference between seasonally averaged BRDF shape and BRDF shape of a particular day may also introduce AOD retrieval error. MODIS BRDF retrieval error is also a major source of uncertainty, which is extreme large at backscattering position.

ACPD
11, 12519–12560, 2011

The retrieval algorithm is based on an assumption that surface BRDF is relative stable from day to day. If the surface BRDF is unstable, large AOD error may occur. This is especially serious at Bondville, where both MAIAC and GASP have large retrieval errors compared to AERONET. We found that at Bondville site the surface BRDF changes rapidly during the period between March and June, when there is no vegetation there. During that period, there are raining days from time to time and the surface changes between wet and dry from day to day, which introduces instability of surface reflectance. Since the western US has much less precipitation, BRDF has less variation from time to time. This is probably the reason that AOD retrievals are more accurate at the two western sites than those at the eastern sites.

Figure 11 shows the diurnal variations of the average errors of AOD retrievals with standard deviation as error bar. The patterns vary from site to site. We don't observe any apparent pattern at the three eastern sites. However, at the other three sites, i.e. Bondville, Railroad Valley, and UCSB, we found that the errors are larger at noon than in the morning and in the afternoon.

4.2.4 Non-Lambertian effect

We use non-Lambertian SHARM radiative transfer model in our retrieval, which may introduce AOD retrieval difference from the retrievals using radiative transfer models that assumes Lambertian surface. To analyze the AOD retrieval difference between using non-Lambertian model and using Lambertian model, we calculate the diurnal variations of the TOA reflectance at GSFC and Railroad Valley using typical values of surface BRDF at these two sites, shown in Fig. 12. GSFC site is located in the eastern US in Maryland state and surface BRDF peaks at local noon due to the sun-satellite geometry. Railroad Valley is located in the western US in Nevada and the surface reflectance is high in the morning and decreases during the day time. In both sites, we can see that the TOA reflectance is overestimated at high surface BRDF geometry and underestimated at low surface BRDF geometry. If Lambertian surface is assumed, AOD will be underestimated at noon at GSFC and in the morning at Railroad Valley and

ACPD
11, 12519–12560, 2011

will be overestimated in the early morning and in the late afternoon at GSFC and in the afternoon at Railroad Valley. At GSFC site, the differences of TOA reflectance between the two surface assumptions are about 0.05 at AOD 0.5 and 1.0, and about 0.02 at AOD close to 0 at noon when the differences are large. Such differences can introduce underestimates of AOD 0.15 for AOD equal to 0.5 and 1.0 and introduce underestimate of AOD 0.05 if AOD is close to 0. At Railroad Valley, we don't have retrievals in the morning because of the high surface reflectance caused uncertainty discussed in the previous sections. The AOD retrievals are more sensitive to the surface assumption in the early afternoon than in the late afternoon. At 2015 UTC, Lambertian assumption can cause 0.07, 0.2, and 0.25 error for AOD at 0, 0.5, and 1.0, respectively. At 2215 UTC, Lambertian assumption can introduce 0.03, 0.1, and 0.18 error for AOD at 0, 0.5, and 1.0, respectively. In both time instances, the AOD retrievals are overestimated if Lambertian surface is assumed. From the analysis above, we may introduce an AOD retrieval error as large as 15–20% in some sun-satellite geometry if we use a Lambertian surface assumption. However, error of such magnitude is small compared to other error sources such as surface reflectance and cloud contamination. From the scatter plots shown above, the AOD retrieval error is about 0.2 for AOD close to 0, which is much larger than the error from using Lambertian model. Therefore, the improvement through using the non-Lambertian radiative transfer model is small and do not show a big influence in the scatter plots comparisons between MAIAC and GASP.

4.3 Evaluation of surface reflectance retrievals

The benefit of MAIAC algorithm is the potential of improving the accuracy of the surface reflectance retrievals. This is achieved by reducing the number of days used in the time sequence for the surface reflectance retrieval, and also by abandoning the assumption of AOD = 0.02 in the second clearest day, which is used in GASP surface reflectance retrieval. The retrieval of surface reflectance over a block can usually be obtained by a sequence of cloud free images from the same day if more than three such images

ACPD
11, 12519–12560, 2011

are found for this block. AOD at the clearest observation time is retrieved using time sequence analysis. However, two new assumptions are made in such retrievals: the BRDF shape of GOES channel 1 is proportional to that derived from MODIS 2.12 µm channel, and the BRDF shape does not have large variation during a season. The accuracy of such assumptions and the accuracy of MODIS 2.12 µm BRDF retrievals should have direct effect on the accuracy of GOES surface reflectance retrievals and hence the accuracy of AOD retrievals.

To evaluate the accuracy of the surface reflectance, we use the GOES channel 1 TOA reflectance and AERONET AOD together with LUT to correct the atmosphere effect and obtain estimation of the surface BRDF at the AERONET sites. This method was also used previously by Hauser et al. (2005), Knapp et al. (2005), and Popp et al. (2007) and its accuracy is affected by cloud and cloud shadow contamination.

Figure 13 shows the BRDF retrieval errors at two AERONET sites, i.e. GSFC and Railroad Valley, vs. UTC time. To compare MAIAC and GASP, the data shown have one-to-one correspondence between MAIAC and GASP. At GSFC site, both MAIAC and GASP appear to have similar error magnitudes and variations. At Railroad Valley, because surface BRDF is high and the TOA reflectance is not sensitive to AOD during the morning and noon, the retrievals are only available in the afternoon. MAIAC BRDF retrievals are more accurate than GASP BRDF retrievals at Railroad Valley site. We can notice that GASP tends to underestimate surface BRDF there. To understand the causes of the surface retrieval errors in GASP and the benefit of MAIAC algorithm, we plot in Fig. 14 time series of surface reflectance at GSFC (1915 UTC) and Railroad Valley (2215 UTC). The surface reflectance is not a constant over time. The variation of surface reflectance is less at GSFC than at Railroad Valley. At GSFC, the surface reflectance has a down trend in the testing period. Since GASP retrieval picks second darkest in 28-day period, it tends to select the latest surface reflectance. Therefore, GASP algorithm does not have large bias. Although using MAIAC can reduce the time period for surface retrieval, such benefit does not show at GSFC site for the period of test. However, the situation is different at Railroad Valley site. We observe high

ACPD
11, 12519–12560, 2011

frequency of variation in surface reflectance with large range. Using GASP, surface reflectance retrieved tends to be at the lower bound of the time series. Also, during day 100 to 200, the uptrend of the time series induces GASP to select the earliest surface reflectance within the 28-day period. Due to this reason, we observe underestimates of surface reflectance in GASP around 0.03. Since MAIAC retrieval does not select the dark pixels in the time series, it does not have such tendancy to retrieve lower bound of the surface reflectance and its retrievals are between the lower bound and the upper bound. In addition, MAIAC uses a short period of time for surface retrieval. It does not suffer from the long term tendancy of surface reflectance variation.

4.4 Other sources of errors

Besides surface reflectance, there are other sources of AOD retrieval errors, including calibration, cloud contamination, aerosol model, etc. GOES visible channel uses vicarious calibration methods (http://www.star.nesdis.noaa.gov/smcd/spb/fwu/homepage/GOES_Imager_Vis_OpCal.php). The methods include star-based calibration, lunar-based calibration, deep convection cloud calibration, desert-based calibration, GOES-GOME inter-calibration, calibration using MODIS. The calibration methods estimate the degradation rate of GOES visible channel sensor. From the difference between the different calibration methods, we can estimate that the calibration error is about 5%. However, since surface BRDF is also derived from the same calibration, the error from the calibration tends to be lower since both surface BRDF and TOA reflectance are biased similarly.

Cloud contamination is another source of error. We have made efforts to improve cloud masks, such as applying threshold for standard deviation in 3×3 pixels box. However, we still cannot eliminate the subpixel scale cloud and thin cirus cloud, which can generate overestimated AOD.

Because we only have one visible channel to be used for aerosol retrieval, we do not have the degree of freedom to select aerosol models and therefore we use a single aerosol model in the retrieval. In reality, aerosol model can change and thus

ACPD
11, 12519–12560, 2011

cause AOD retrieval error. To estimate such error, we calculated TOA reflectance using biomass burning model and dust model at different geometries and compare against the one used in MAIAC. We find that the error from using wrong aerosol model can be as high as 25%.

When AOD is small, the AOD retrieval error originating from calibration and aerosol model is also small, i.e. the error approaches 0 if AOD is close to 0. Both GASP and MAIAC uses similar cloud mask schemes, the difference between them at small AOD should be mainly originated from the differences in their surface reflectance retrievals. The difference is apparent at the two western sites as seen in Fig. 10. For example, at Railroad Valley, the intercept is 0.1 for GASP vs. AERONET AOD, and it is −0.01 for MAIAC vs. AERONET AOD. At the four other sites in the eastern and central US, the differences are small.

4.5 A regional retrieval example

In this section, we demonstrate a regional retrieval example using the MAIAC algorithm for a California fire case in July, 2008. Figure 15 shows an example of California fire AOD retrievals from MAIAC, GASP, Terra and Aqua on 10 July 2008. MAIAC AOD retrievals demonstrate much better quality than those from GASP and MODIS. The AOD data coverage from MAIAC is larger than GASP because MAIAC uses a different screen algorithm for high reflectance surface, which is described in the previous section. Because of high surface reflectance over this area and MODIS uses dark pixels for AOD retrieval, MODIS AOD maps also show large areas without retrieval. MAIAC AOD map shows more detailed smoke plume structures than MODIS AOD map because of the higher spatial resolution. MAIAC AOD retrievals are also sensitive to surface reflectance and they have larger errors when surface reflectance is high. In the western US, the surface reflectance is high in the morning and low in the afternoon if the area is viewed from the GOES-12 satellite position. Hence the accuracy of the AOD retrievals for the western US is high in the afternoon for GOES-12.

ACPD
11, 12519–12560, 2011

Figure 16 shows the scatter plot of the AOD retrievals from MAIAC vs. those from MODIS Aqua. GASP AOD vs. MODIS Aqua AOD scatter plot is also shown for comparison. GOES AOD used here was taken from the retrievals at 2015 UTC, which is closest to the overpass time of Aqua. MAIAC AOD has a good correlation of 0.87 with MODIS Aqua and it is better than that between GASP AOD and MODIS AOD. MAIAC AOD shows lower retrieval values than MODIS AOD with a slope of 0.56. This is reasonable since MODIS AOD was found to overestimate in the southwest region of US (Drury et al., 2008).

5 Conclusions

We developed a new AOD retrieval algorithm by modifying the MAIAC algorithm for MODIS. In this algorithm, seasonally averaged MODIS surface BRDF in the 2.1 µm band is used along with the GOES visible channel for the retrieval of surface reflectance and AOD. This algorithm can retrieve surface reflectance using GOES images from a much shorter period of time than the operational GASP algorithm, which uses 28-day composites to obtain surface reflectance. The algorithm is validated by comparing with the AERONET and GASP AOD retrievals at six AERONET sites across continental US. MAIAC AOD compares good with AERONET AOD at two western US sites, i.e. Railroad Valley and UCSB, and is better than GASP retrievals at these sites. At the other four eastern and central sites, MAIAC algorithm has similar retrieval accuracy with GASP. This is probably due to the relative large variations of surface BRDF caused by the precipitation and vegetation change in the eastern and central area. The precipitation and vegetation change is much less in the western US so that surface BRDF is relatively stable from day to day. Hence, we expect MAIAC algorithm be especially suitable for arid areas where the BRDF. MODIS BRDF retrieval error can introduce large errors in MAIAC retrieval. This is extremely serious at backscatter position, caused by the different sampling geometry between MODIS and GOES, hence we filter out the AOD retrievals at such geometry. Such problem will not exist if MAIAC algorithm is

ACPD
11, 12519–12560, 2011

applied to the data from GOES-R satellite, which is planned to be launched in 2015. GOES-R ABI (Advanced Baseline Imager) (Schmit et al., 2005) contains blue, red and SWIR (2.12 µm) channels similar to those of MODIS. Using this data, 2.12 µm BRDF can be retrieved directly without using seasonal average BRDF.

Acknowledgements. This work is supported by the NOAA GOES-R risk reduction program grant NA08NES4280023.

References

Al-Saadi, J., Szykman, J., Pierce, R. B., Kittaka, C., Neil, D., Chu, D. A., Remer, L., Gumley, L., Prins, E., Weinstock, L., MacDonald, C., Wayland, R., Dimmick, F., and Fishman, J.: Improving National Air Quality Forecasts with Satellite Aerosol Observations, Bull. Am. Met. Soc., 86, 1249–1261, 2005. 12521

Anderson, T. L., Charlson, R. J., Winker, D. M., Ogren, J. A., and Holmen, K.: Mesoscale variations of tropospheric aerosols, J. Atm. Sci., 60, 119–136, 2003. 12525

Charlson, R. J., Schwartz, S. E., Hales, J. M., Cess, R. D., Coakley, J. A., Hansen, J. E., and Hoffman, D. J.: Climate forcing by anthropogenesis aerosols, Science, 255, 423–430, 1992. 12520

Chow, J. C., Watson, J. G., Mauderly, J. L., Costa, D. L., Wyzga, R. E., Vedal, S., Hidy, G. M., Altshuler, S. L., Marrack, D., Heuss, J. M., Wolff, G. T., Pope, C. A. III, and Dockery, D. W.: Health effects of fine particulate air pollution: lines that connect critical review discussion, J.Air & Waste Manage. Assoc., 56, 1368–1380, 2006. 12521

GOES I-M databook, http://goes.gsfc.nasa.gov/text/goes.databook.html, 1996, accessed 9 June, 2009. 12526

Deuzé, J. L., Bréon, F. M., Devaux, C., Goloub, P., Herman, M., Lafrance, B., Maignan, F., Marchand, A., Nadal, F., Perry, G., and Tanré, D.: Remote sensing of aerosol over land surfaces from POLDER-ADEOS-1 polarized measurements, J. Geophys. Res., 106(D5), 4913–4926, doi:10.1029/2000JD900364, 2001. 12521

Drury, E., Jacob, D. J., Wang, J., Spurrs, R. J. D., and Chance, K.: Improved algorithm for MODIS satellite retrievals of aerosol optical depths over land, J. Geophys. Res., 113, D16204, doi:10.1029/2007JD009573, 2008. 12539

ACPD

11, 12519–12560, 2011

Fraser, R. and Kaufman, Y. J.: The relative importance of aerosol scattering and absorption in remote sensing, Trans. Geosci. Remote Sens., GE-23(5), 625–633, 1985. 12532
Hauser, A., Oesch, D., Foppa, N., and Wunderle, S.: NOAA AVHRR derived aerosol optical depth over land, J. Geophys. Res., 110, D08204, doi:10.1029/2004JD005439, 2005. 12536
Heidinger, A. K., Anne, V. R., and Dean, C.: Using MODIS to estimate cloud contamination of the AVHRR data record, J. Atmos. Oceanic Technol., 19, 586–601, 2001. 12523
Critical review discussion: Remote sensing of particulate pollution from space: Have we reached the promised land?, J. Air. Waste Manage. Assoc., 59, 1130–1139, doi:10.3155/1047-3289.59.10.1130, 2009. 12521
Hoff, R. M., Christopher, S. A., Critical Review – Remote sensing of particulate pollution from space: Have we reached the promised land? A critical review, J. Air. & Waste Manage. Assoc., 2009, 59, 645–675, doi:10.3155/1047-3289.59.6.645, 2009. 12521
Holben, B. N., Eck, T. F., Slutsker, I., Tanré, D., Buis, J. P., Setzer, A., Vermote, E., Reagan, J. A., Kaufman, Y. J., Nakajima, T., Lavenu, F., Jankowiak, I., and Smirnov, A.: AERONET: A federated instrument network and data archive for aerosol characterization, Remote Sens. Environ., 66, 1–16, 1998. 12524
Intergovernmental Panel on Climate Change: Climate Change 2007: The Physical Science Basis, Cambridge Univ. Press, Cambridge, UK, 2007. 12521
Kaufman, Y. J.: Satellite sensing of aerosol absorption, J. Geophys. Res., 92(D4), 4307–4317, 1987. 12532
Kaufman, Y. J., Tanré, D., Remer, L. A., Vermote, E. F., Chu, D., and Holben, B. N.: Operational remote sensing of tropospheric aerosol over the land from EOS-MODIS, J. Geophys. Res., 102(D14), 17051–17061, 1997. 12521
Kiehl, J. T. and Briegleb, B. P.: The radiative roles of sulfate aerosols and greenhouse gases in climate forcing, Science, 260, 311–314, 1993. 12521
Knapp, K., Von der Haar, T., and Kaufman, Y.: Aerosol optical depth retrieval from GOES-8: uncertainty study and retrieval validation over South America, J. Geophys. Res., 107(D7), 4055, doi:10.1029/2001JD000505, 2002. 12529
Knapp, K. R., Frouin, R., Kondragunta, S., and Prados, A.: Toward aerosol optical depth retrievals over land from GOES visible radiances: determining surface reflectance, Int. J. Remote Sens., 26(18), 4097–4116, doi:10.1080/01431160500099329, 2005. 12523, 12536
Levy, R.C., Remer, L. A., Mattoo, S., Vermote, E. F., and Kaufman, Y. J.: Second-generation operational algorithm: retrieval of aerosol properties over land from inversion of Moderate

ACPD
11, 12519–12560, 2011

Resolution Imaging Spectroradiometer spectral reflectance, J. Geophys. Res., 112, D13211, doi:10.1029/2006JD007811, 2007. 12521, 12524
Lucht, W., Schaaf, C. B., and Strahler, A. H.: An algorithm for the retrieval of albedo from space using semiempirical BRDF models, IEEE Trans. Geosci. Remote Sens., 38, 977–998, 2000. 12524
Lyapustin, A. and Knyazikhin, Y.: Green's function method in the radiative transfer problem. I: Homogeneous non-Lambertian surface, Appl. Optics, 50, 3495–3501, 2001. 12528
Lyapustin, A. and Wang, Y.: Parameterized code Sharm-3D for radiative transfer over inhomogeneous surfaces, Appl. Optics, 55, 7602–7610, 2005. 12528
Lyapustin, A. and Wang, Y.: MAIAC: multi-angle implementation of atmospheric correction for MODIS, algorithm theoretical basis document (ver. 1.0), 2008. 12528, 12529
Lyapustin, A., and Wang, Y. : The time series technique for aerosol retrievals over land from MODIS, in: Satellite aerosol remote sensing over land, edited by: Kokhanovky, A. and De Leeuw, G., 69–99, Springer Praxis Books ISBN 978-3-540-69396-3, 2009. 12522
Martins, J. V., Tanré, D., Remer, L., Kaufman, Y., Mattoo, S., and Levy, R.: MODIS Cloud screening for remote sensing of aerosols over oceans using spatial variability, Geophys. Res. Lett., 29(12), 8009, doi:10.1029/2001GL013252, 2002. 12527
Martonchik, J. V., Diner, D. J., Kahn, R. A., Ackerman, T. P., Verstraete, M. E., Pinty, B., and Gordon, H. R.: Techniques for the retrieval of aerosol properties over land and ocean using multiangle imaging, IEEE Trans. Geosci. Remote Sens., 36(4), 1212–1227, 1998. 12521
Pope, C. A., III, Burnett, R. T., Thun, M. J., Calle, E. E., Krewski, D., Ito, K., and Thurston, G. D.: Lung cancer, cardiopulmonary mortality and long-term exposure to fine particulate air pollution, J. Amer. Med. Assoc., 287, 1132–1141, 2002. 12521
Pope, C. A. III and Dockery, D. W.: Health effects of fine particulate air pollution: lines that connect, J. Air. Waste Manage. Assoc., 56, 709–742, 2006. 12521
Popp, C., Hauser, A., Foppa, N., and Wunderle, S.: Remote sensing of aerosol optical depth over central Europe from MSG-SEVIRI data and accuracy assessment with ground-based AERONET measurements, J. Geophys. Res., 112, D24S11, doi:10.1029/2007JD008423, 2007. 12536
Prados, A. I., Kondragunta,S., Ciren,P., and Knapp,K. R.: GOES Aerosol/Smoke Product (GASP) over North America: Comparisons to AERONET and MODIS observations, J. Geophys. Res., 112, D15201, doi:10.1029/2006JD007968,2007. 12521, 12523, 12530
Roujean, J.-L., Leroy, M., and Deschamps, P.Y.: A bidirectional reflectance model of the Earth's

ACPD
11, 12519–12560, 2011

surface for the correction of remote sensing data, J.Geophys.Res., 97, 20455–20468, 1992. 12524

Schmit, T. J., Gunshor, M. M., Menzel, W. P., Gurka, J. J., Li, J., and Bachmeier, A. S.: Introducing the Next-generation Advanced Baseline Imager on GOES-R, Bull. Amer. Meteor. Soc., 86, 1079–1096, 2005. 12540

Stowe, L. L., Davis, P. A., and McClain, E. P.: Scientific basis and initial evaluation of CLAVR-1 global clear/cloud classification algorithm for the advanced very high resolution radiometer, J. Atmos. Oceanic Technol., 16, 656–681, 1999. 12523

Tanré, D., Kaufman, Y. J., Herman, M., and Matteo, S.: Remote sensing of aerosol properties over ocean using the EOS-MODIS spectral radiances, J. Geophys. Res., 102(D14), 16971–16988, 1997. 12521

Vermote, E. F., Tanré, D., Deuzé, J. L., Herman, M., and Morcrette, J. J.: Second simulation of the satellite signal in the solar spectrum, 6S: an overview, IEEE Trans. Geosci. Remote Sens., 35, 675–686, 1997. 12528

Zhang, H., Hoff, R. M., McCann, K., Ciren, P., Kondragunta, S., and Prados, A.: Influence of the ozone and water vapor on the GOES Aerosol and Smoke Product (GASP) retrieval, NOAA Technical report NESDIS 128, 2008. 12529

ACPD

11, 12519–12560, 2011

Table 1. Geographical locations of the AERONET sites.

Site name	Latitude	Longitude
GSFC	38.992° N	76.84° W
Howland	45.2° N	68.733° W
Bondville	40.053° N	88.372° W
Railroad valley	38.504° N	115.962° W
Walker Branch	35.958° N	84.287° W
UCSB	34.415° N	119.845° W

ACPD
11, 12519–12560, 2011

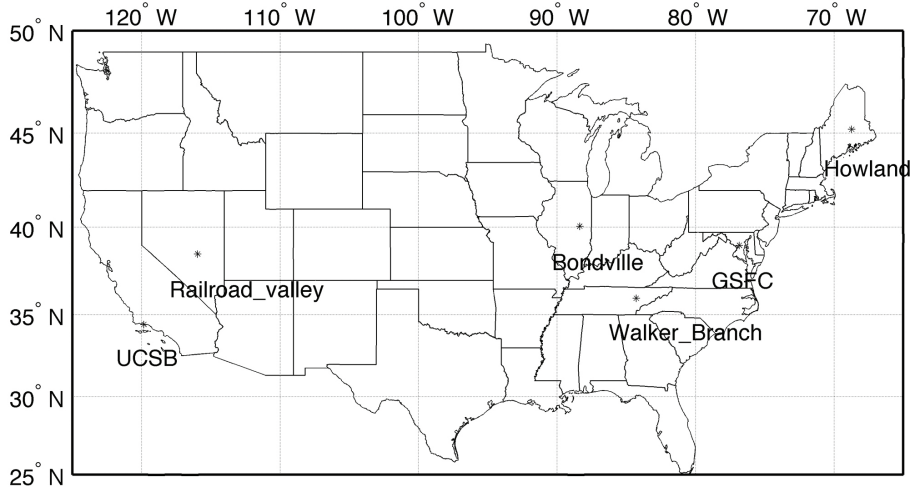

Fig. 1. Locations of the AERONET sites used for validation.

ACPD
11, 12519–12560, 2011

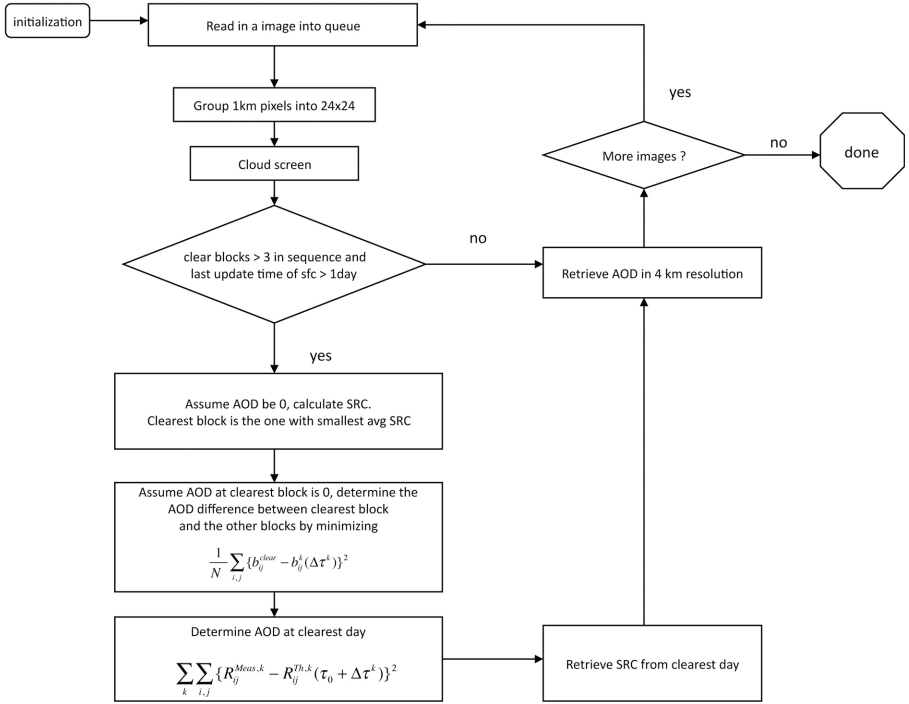

Fig. 2. Flowchart of the MAIAC algorithm for GOES AOD retrieval.

ACPD
11, 12519–12560, 2011

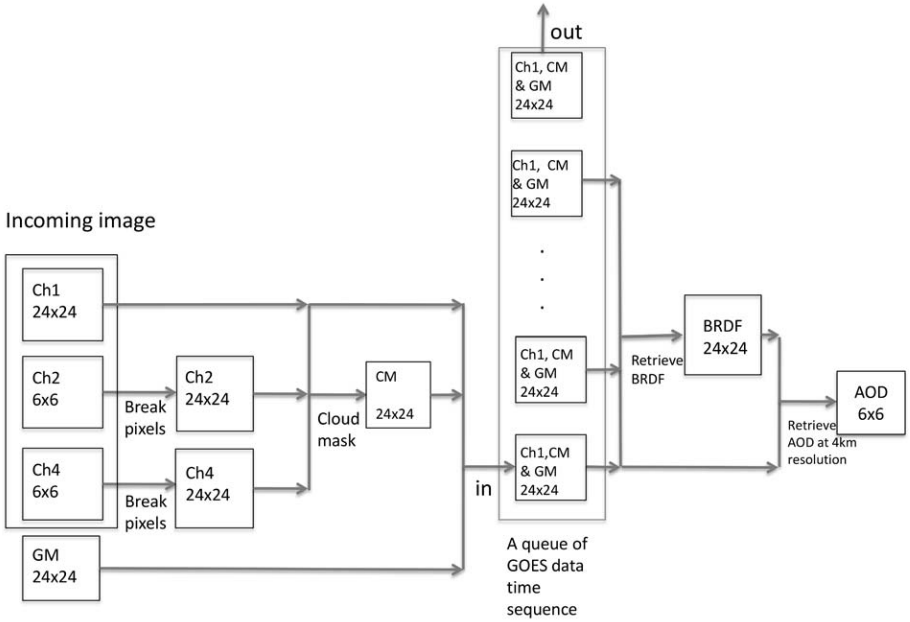

Fig. 3. Data flow in the MAIAC algorithm for GOES AOD retrieval, where ch1, ch2, ch4 represent channel 1, channel 2, channel 4 of GOES data; CM represents cloud mask; GM represents geometry data, including solar zenith angle, view zenith angle, and relative azimuth angle; 24×24, 6×6 represent data block dimensions in pixels. The data blocks all have a size of $24 \times 24\,km^2$, but the number of pixels can be different due to the different resolution, which is the reason that some blocks have dimension of 6×6 in terms of pixels.

ACPD
11, 12519–12560, 2011

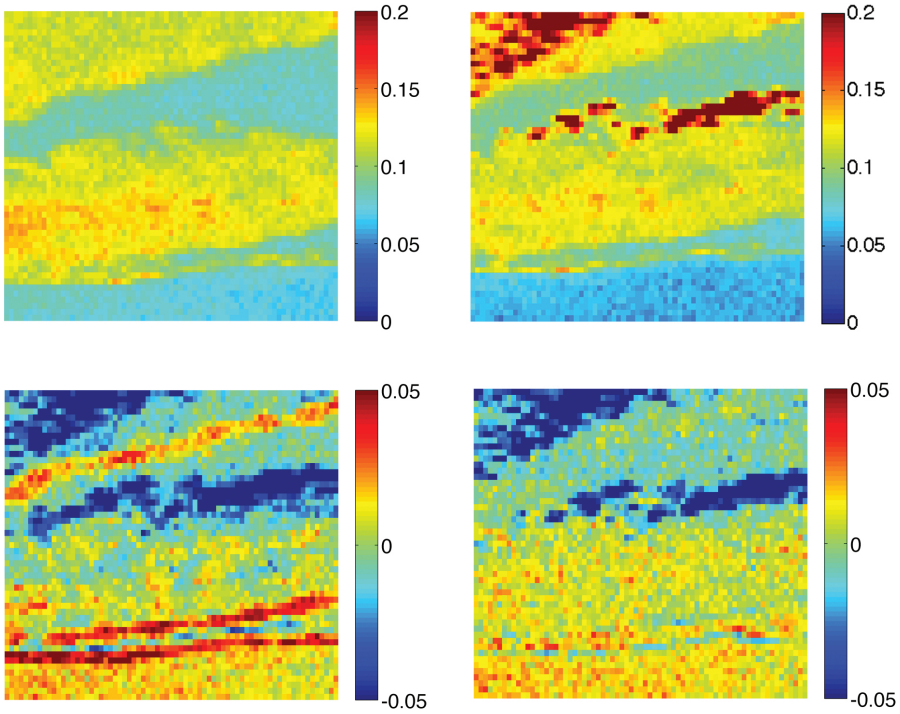

Fig. 4. Image co-registration example. Top: two GOES channel 1 images before registration. Bottom left: subtraction between the two images before registration. Bottom right: subtraction between the two images after registration. The coast lines on the subtraction image show up before registration, which indicate a shift between the two images. The shift is reduced to below one pixel so that the coast lines disappear in the lower right image.

ACPD
11, 12519–12560, 2011

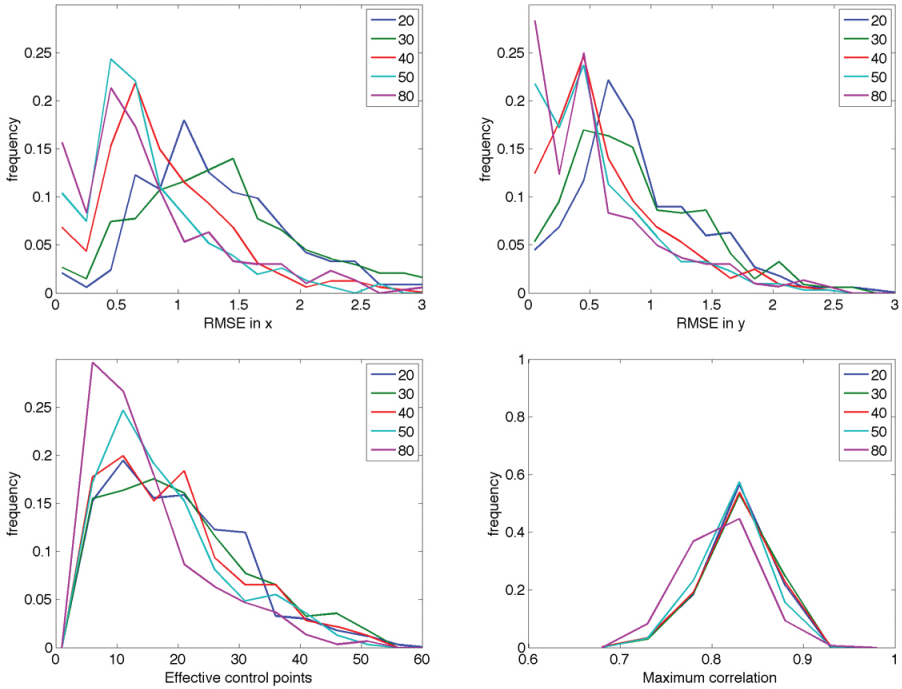

Fig. 5. Statistics of image co-registration with different size of the control points.

ACPD
11, 12519–12560, 2011

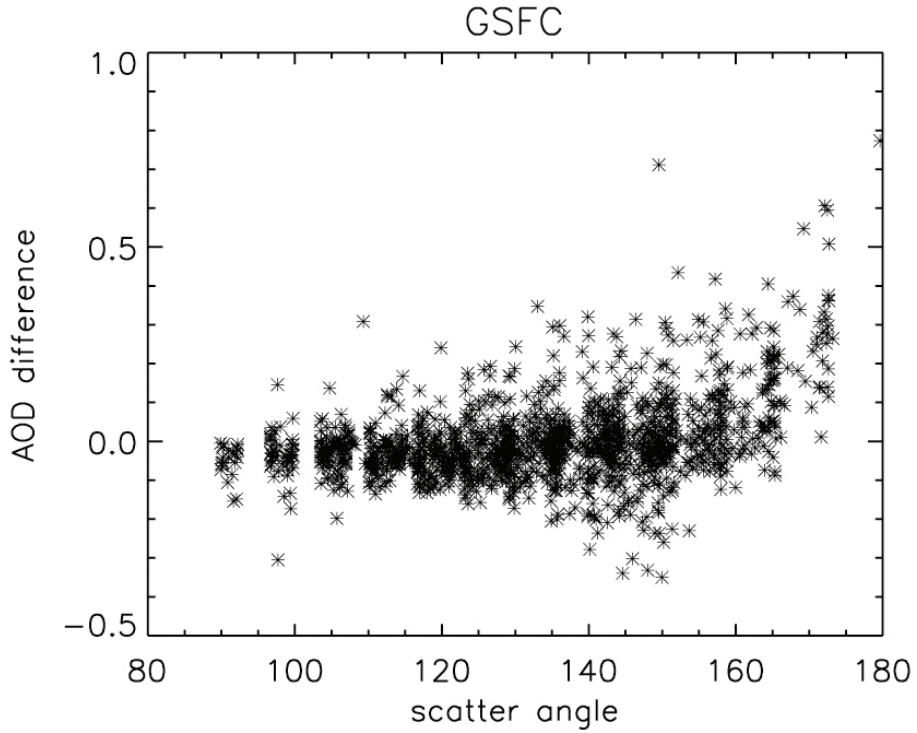

Fig. 6. AOD error vs. scatter angle at GSFC site, where AOD error is defined as GOES AOD minus AERONET AOD.

ACPD
11, 12519–12560, 2011

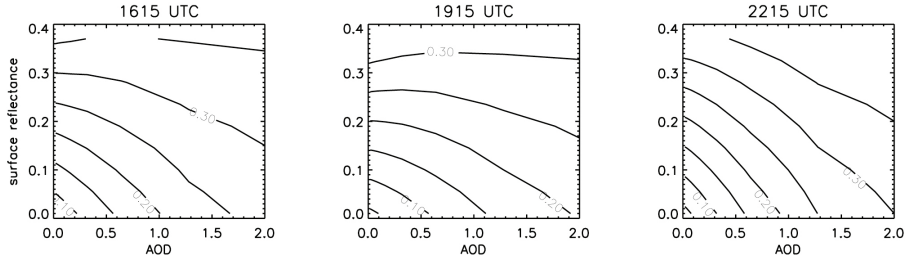

Fig. 7. Contour of TOA reflectance vs surface reflectance and AOD at Railroad Valley site.

ACPD
11, 12519–12560, 2011

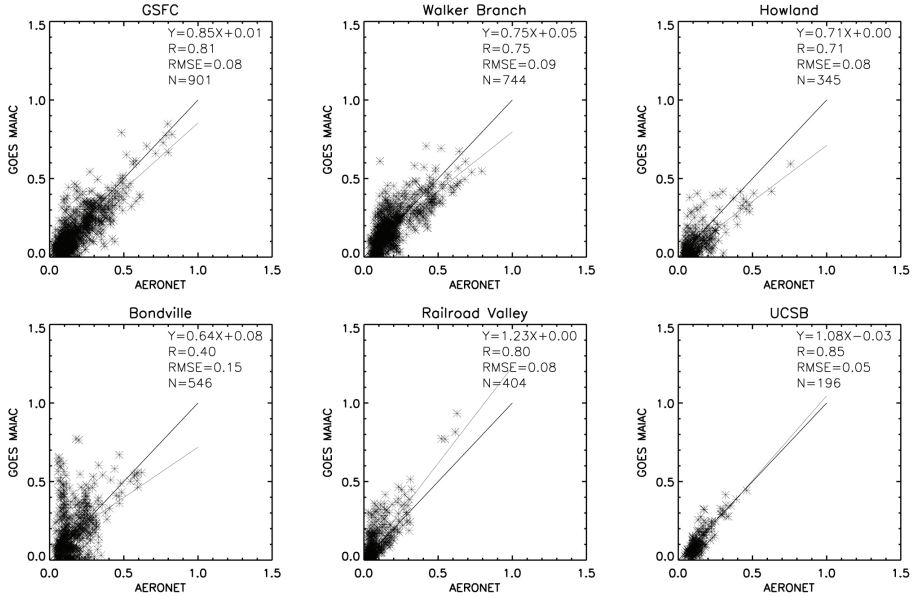

Fig. 8. Scatter plot of MAIAC vs. AERONET AOD.

ACPD
11, 12519–12560, 2011

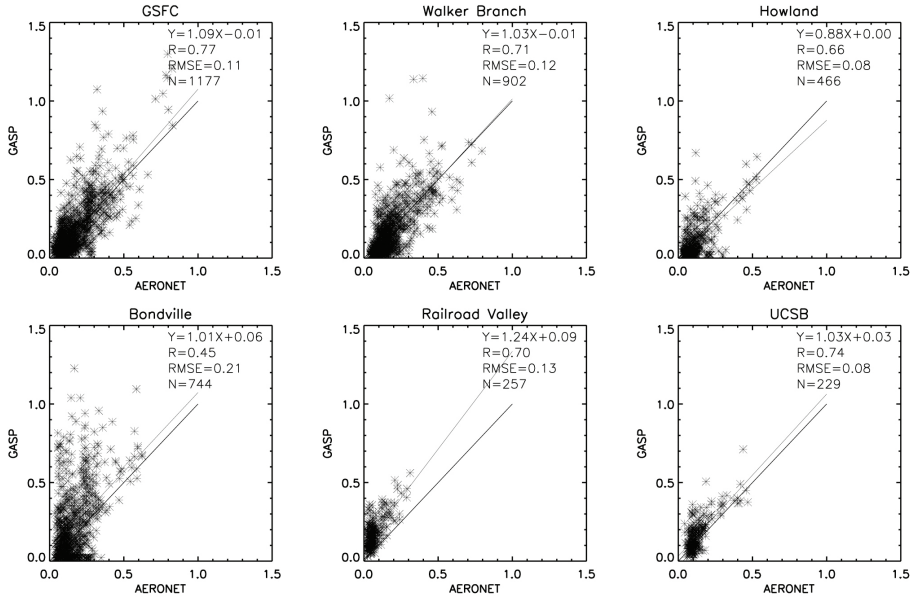

Fig. 9. Scatter plot of GASP vs. AERONET AOD.

ACPD
11, 12519–12560, 2011

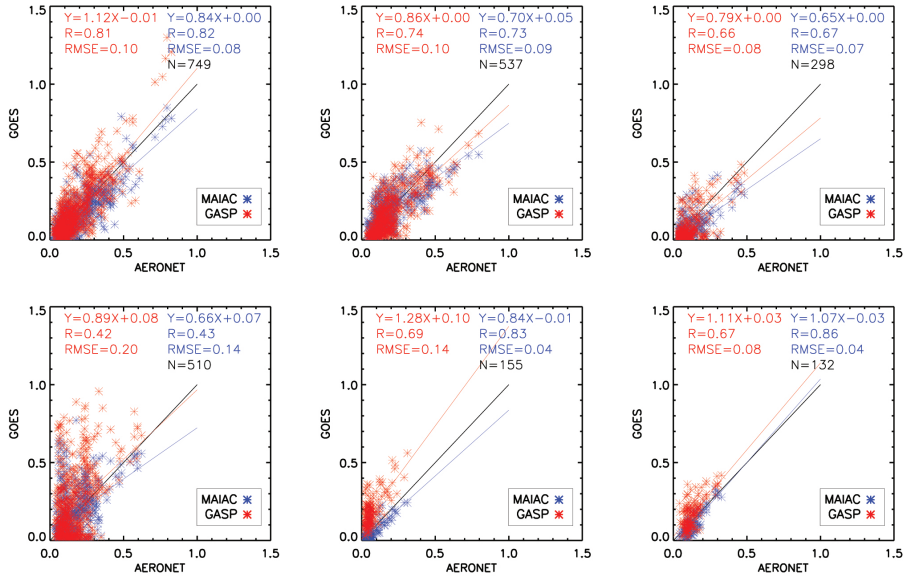

Fig. 10. Scatter plot of MAIAC vs AERONET AOD and GASP vs. AERONET AOD with one-to-one correspondence between MAIAC and GASP retrievals.

ACPD
11, 12519–12560, 2011

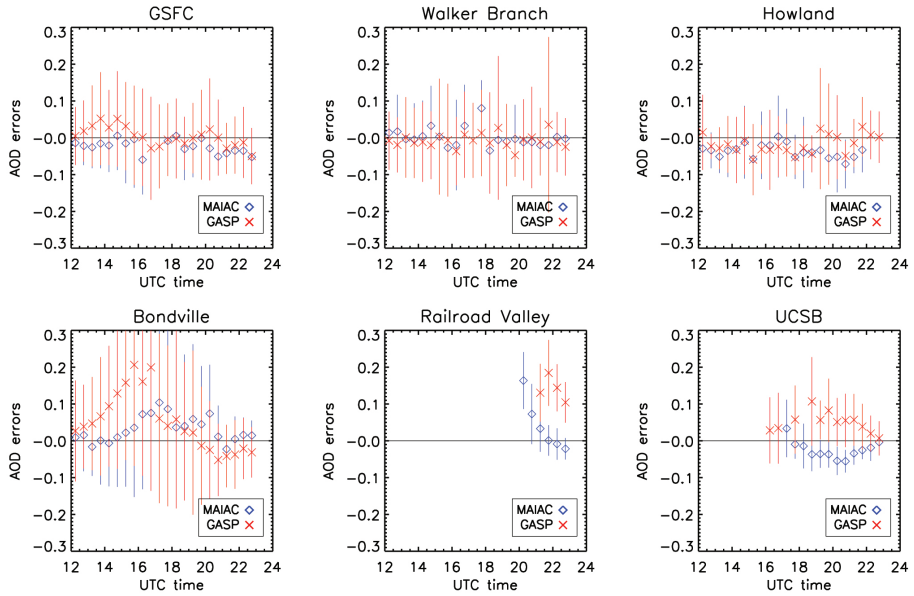

Fig. 11. AOD retrieval errors vs. UTC time. AOD retrieval error is defined as GOES AOD minus AERONET AOD.

ACPD
11, 12519–12560, 2011

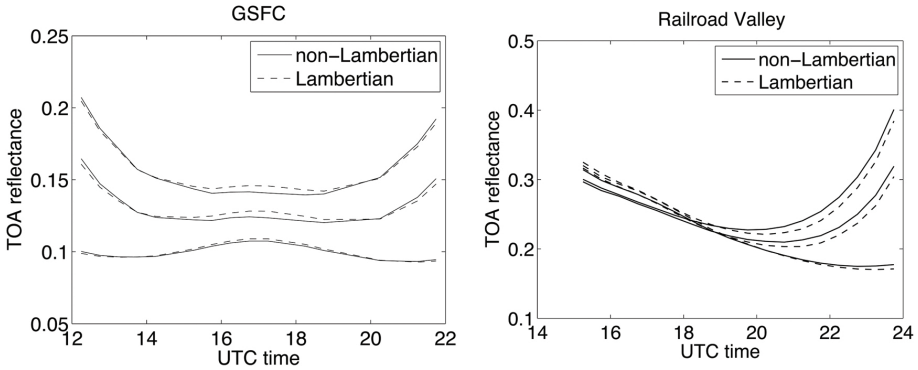

Fig. 12. Comparison of TOA reflectance between Lambertian and non-Lambertian surface at site GSFC and Railroad Valley. The three pairs of lines from bottom to top are calculated using AOD values of 0, 0.5, and 1.0, respectively.

ACPD
11, 12519–12560, 2011

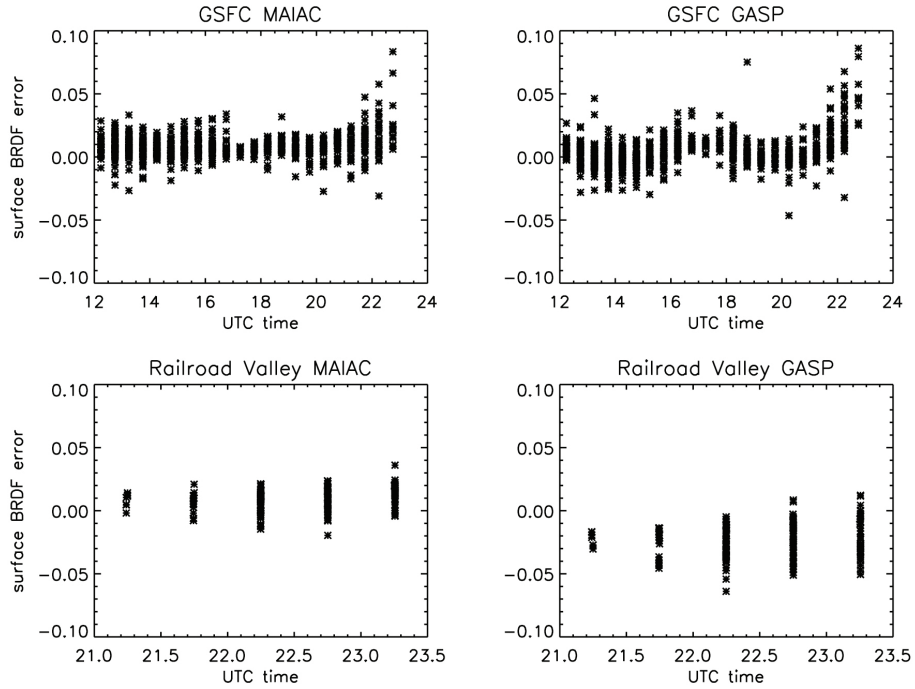

Fig. 13. Surface BRDF error at GSFC and Railroad Valley, which is defined as surface reflectance retrieval from MAIAC or GASP minus surface reflectance retrieval using GOES channel 1 data and AERONET AOD.

ACPD
11, 12519–12560, 2011

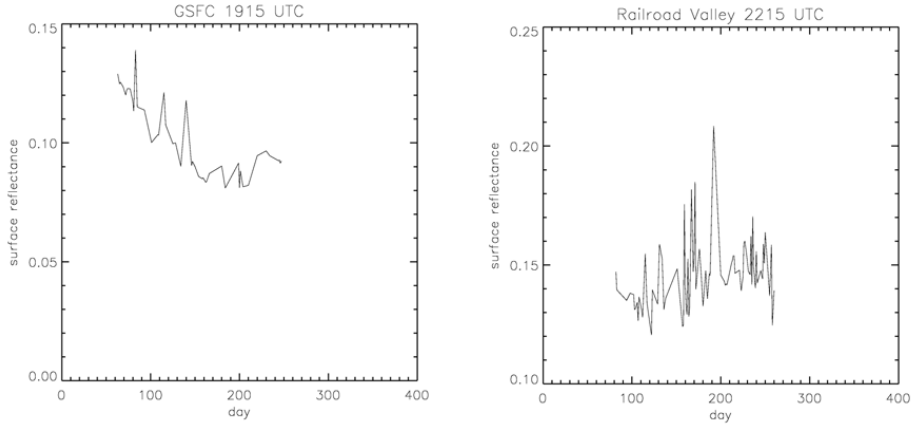

Fig. 14. Surface reflectance timeseries at GSFC (1915 UTC) and Railroad Valley (2215 UTC).

ACPD
11, 12519–12560, 2011

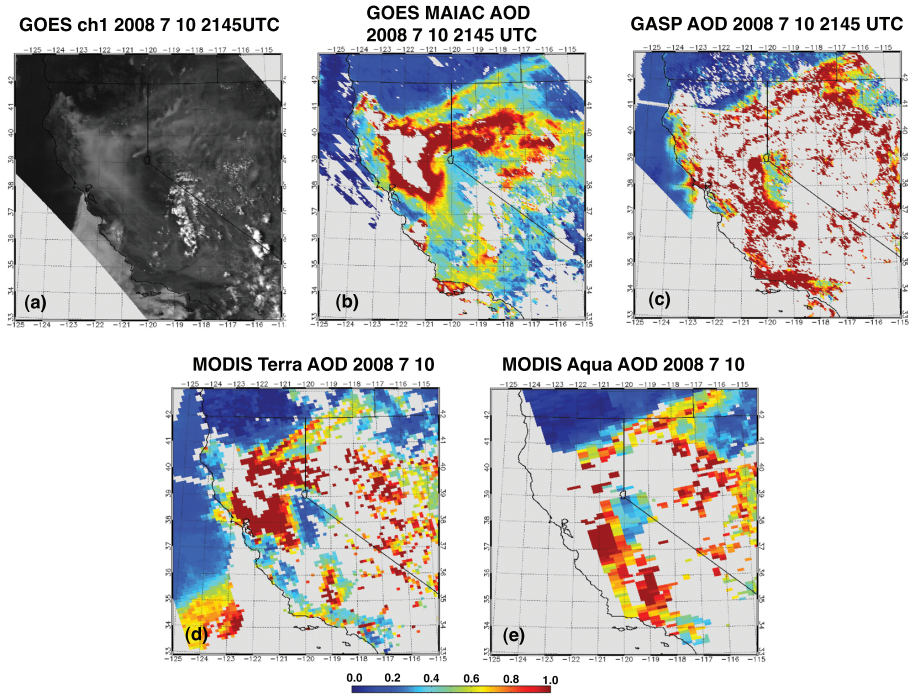

Fig. 15. GOES channel 1 image, AOD retrievals from GOES and MODIS for July 2008 California fire (day 192, 2008). **(a)** GOES channel 1 image; **(b)** MAIAC AOD retrieval; **(c)** GASP AOD retrieval; **(d)** MODIS Terra AOD retrieval; **(e)** MODIS Aqua AOD retrieval.

ACPD
11, 12519–12560, 2011

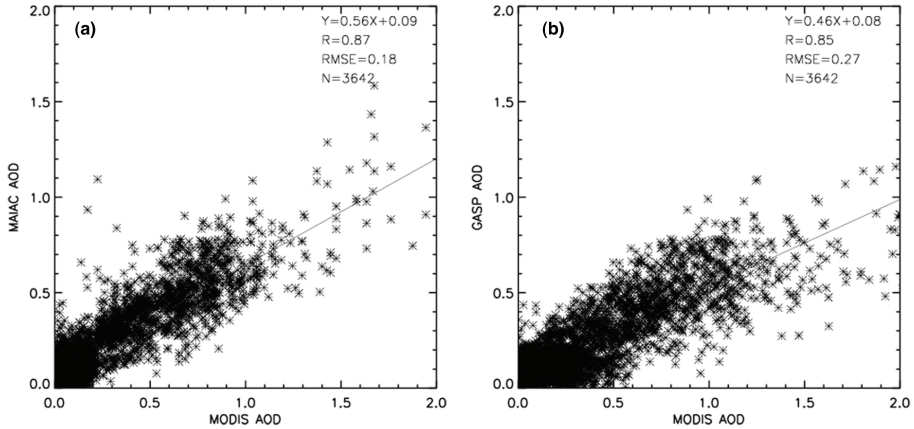

Fig. 16. Scatter plot of GOES AOD vs. MODIS AOD from Aqua for the California fire on 10 July 2008 at Aqua overpass time. **(a)** MAIAC AOD vs MODIS AOD from Aqua; **(b)** GASP AOD vs MODIS AOD from Aqua.

ACPD
11, 12519–12560, 2011